Supplementary Information

Assemblable thermoelectric Lego blocks for reconfigurable, self-healing, and flexible power generators

Keonkuk Kim[1†], Kyuha Park[2†], Jihyang Song[3], Ji Eun Lee[4*], Donghee Son[2,3*], and Jae Sung Son[1*]

[1]*Department of Chemical Engieering, Pohang University of Science and Technology (POSTECH), Gyeongsangbuk-do 37673, Republic of Korea.*

[2]*Department of Electrical and Computer Engineering, Sungkyunkwan University (SKKU), Suwon 16419, Republic of Korea*

[3]*Department of Artificial Intelligence System Engineering, Sungkyunkwan University (SKKU), Suwon 16419, Republic of Korea*

[4]*School of Chemical Engineering, Chonnam National University (CNU), Gwangju 61186, Republic of Korea*

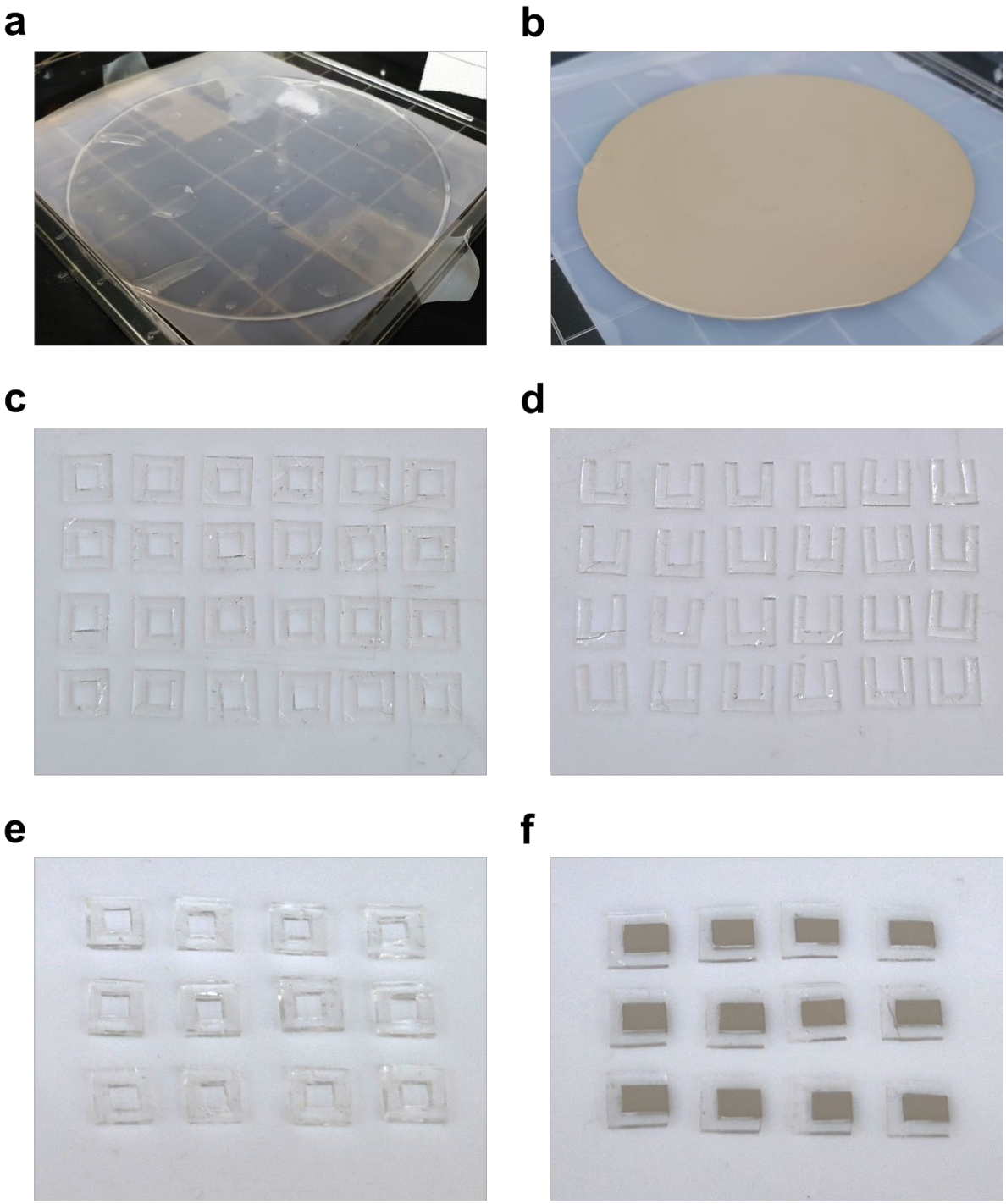

Supplementary Fig. 1 | Photographs of SHP and AgF-SHP samples

Photographs of **a.** as-prepared SHP film, **b.** as-prepared AgF-SHP film, **c.** hollow-squared cut SHP films, **d.** U-shaped cut SHP films, **e.** center part of TE Lego block and **f.** upper and lower electrode part of TE Lego block.

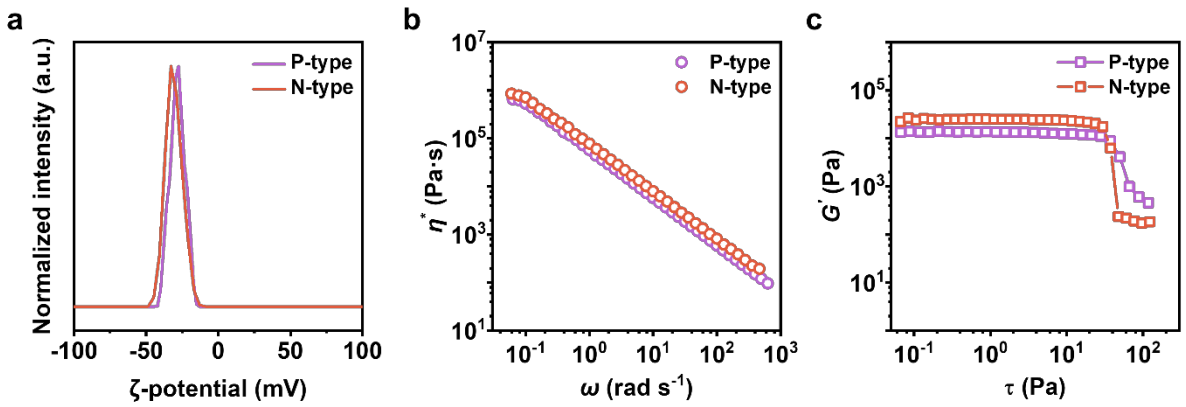

Supplementary Fig. 2 | Characterization of TE 3D printing inks

a. ζ-potential, **b.** Complex viscosity (η^*) dependent on the angular frequency and **c.** Storage moduli (G') dependent on the shear stress of the p-type and n-type TE 3D printing inks

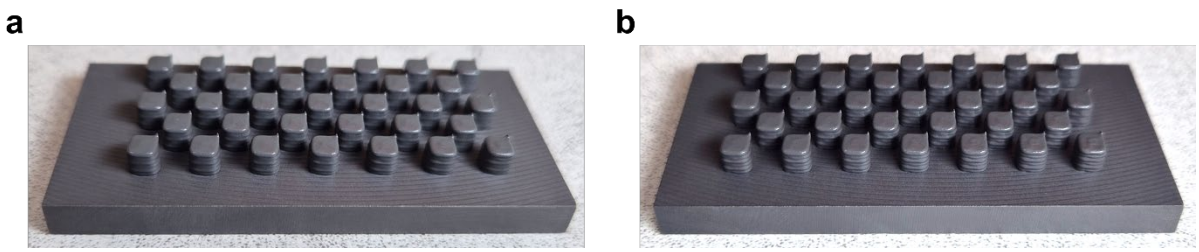

Supplementary Fig. 3 | 3D-printed p-type and n-type TE legs

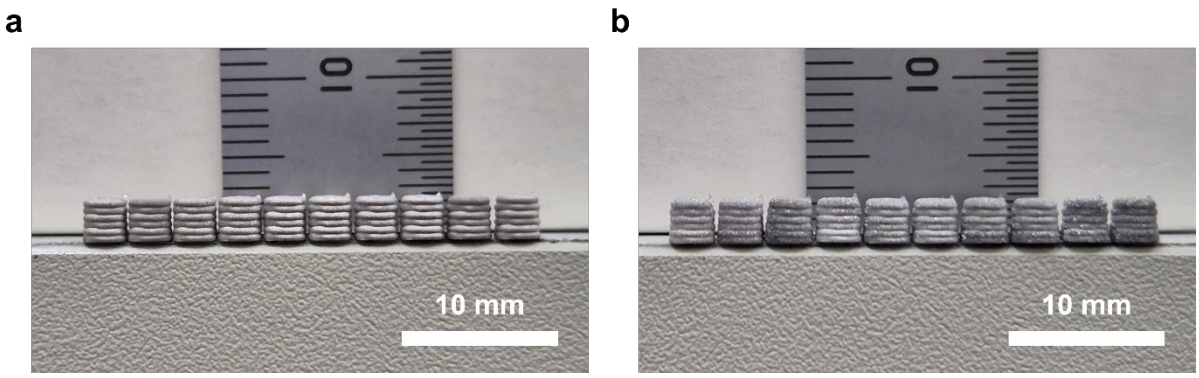

Supplementary Fig. 4 | Volume shrinkage comparison of 3D-printed TE legs

Photographs of the 3D-printed and sintered **a.** p-type and **b.** n-type TE legs by one-step 3D-printing process

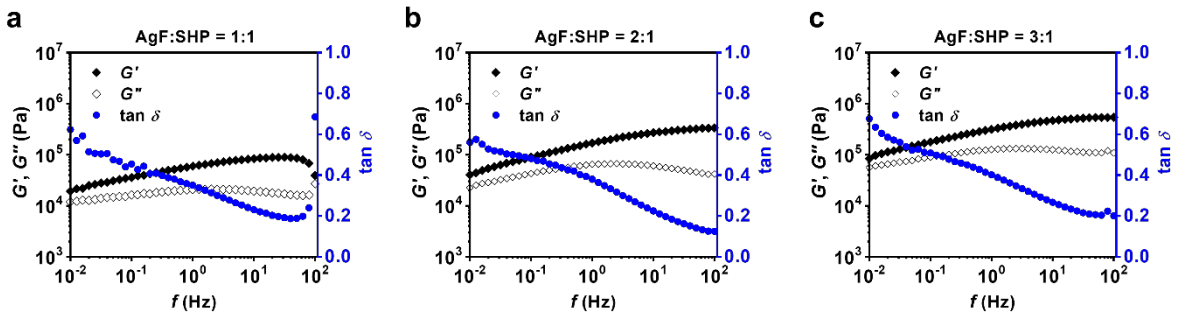

Supplementary Fig. 5 | Rheological properties of AgF-SHP with different weight ratios

Storage modulus (G'), Loss modulus (G''), and tan δ (shown in blue) of **a.** AgF-SHP = 1:1, **b.** AgF-SHP = 2:1, and **c.** AgF-SHP = 3:1 samples, respectively

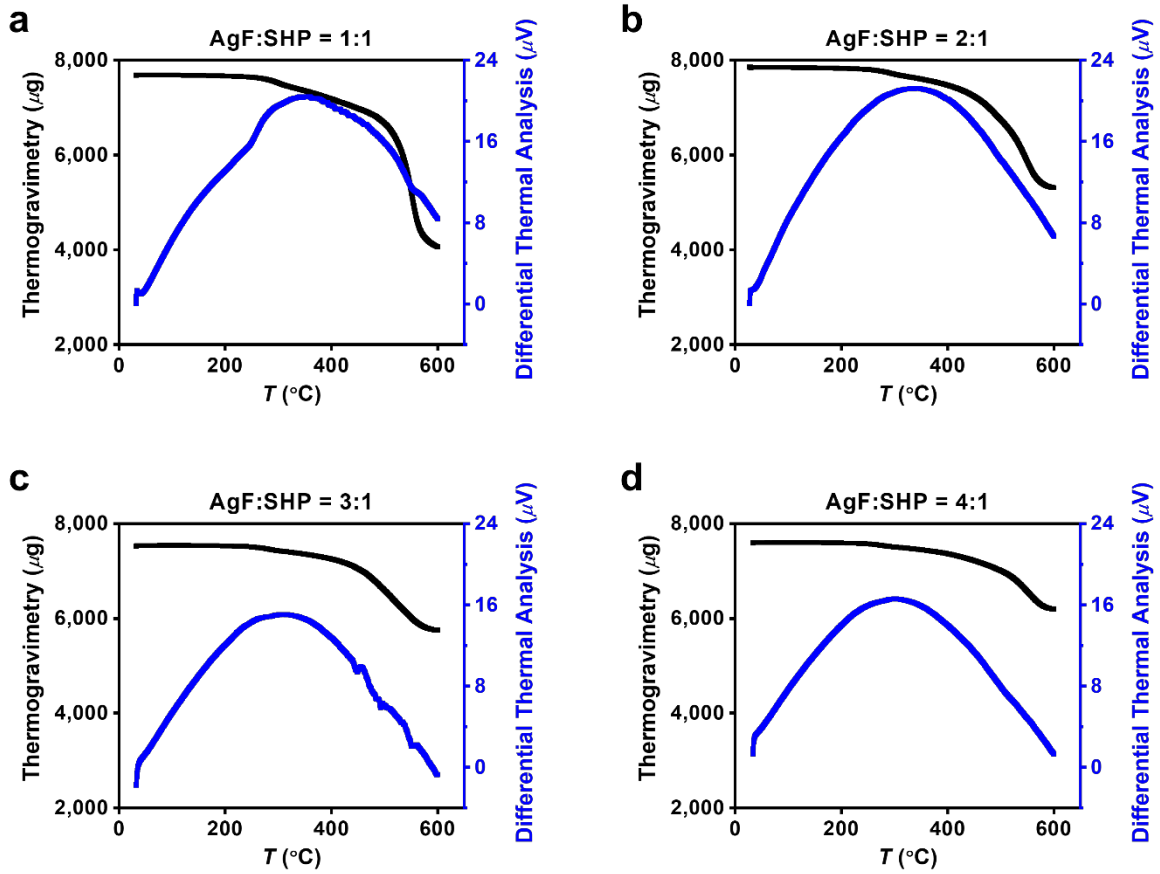

Supplementary Fig. 6 | Temperature-dependent TGA curves of AgF-SHP with varying AgF loading ratios

Continuous weight loss with increasing temperature and differential thermal analysis (DTA, shown in blue) from 0 °C to 600 °C for the AgF-SHP series: **a.** AgF-SHP = 1:1, **b.** AgF-SHP = 2:1, **c.** AgF-SHP = 3:1, and **d.** AgF-SHP = 4:1 samples, respectively

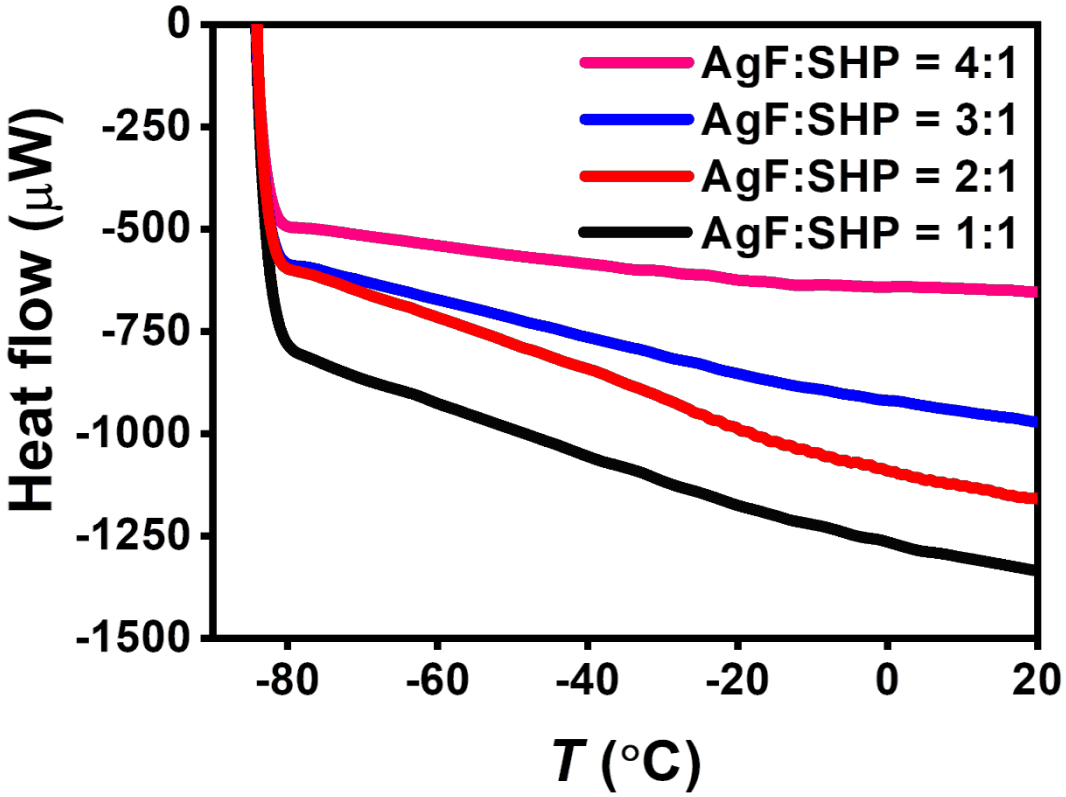

Supplementary Fig. 7 | Temperature-dependent DSC curves of AgF-SHP with varying AgF loading ratios

Heat flow variations as a function of temperature reveal the thermal transitions of the AgF-SHP series in the range of −80 °C to 20 °C

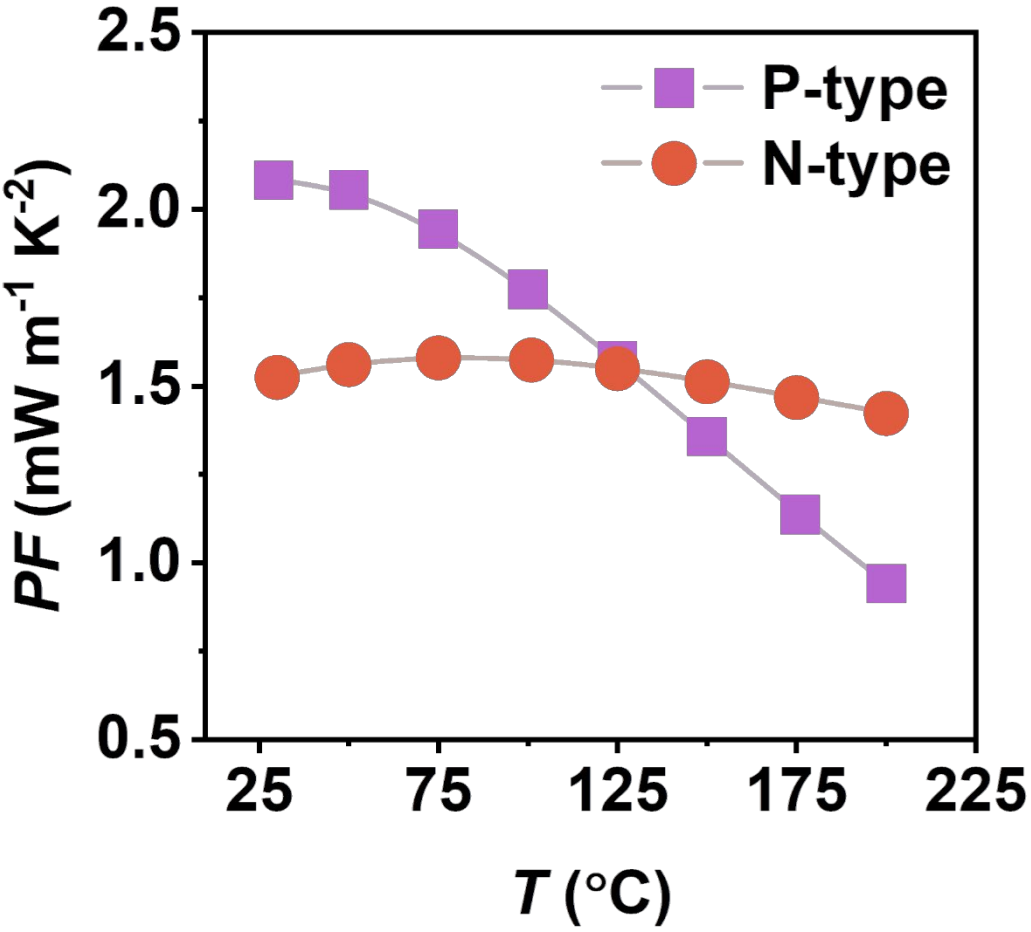

Supplementary Fig. 8 | Temperature-dependent power factor of the 3D-printed p-type and n-type TE materials

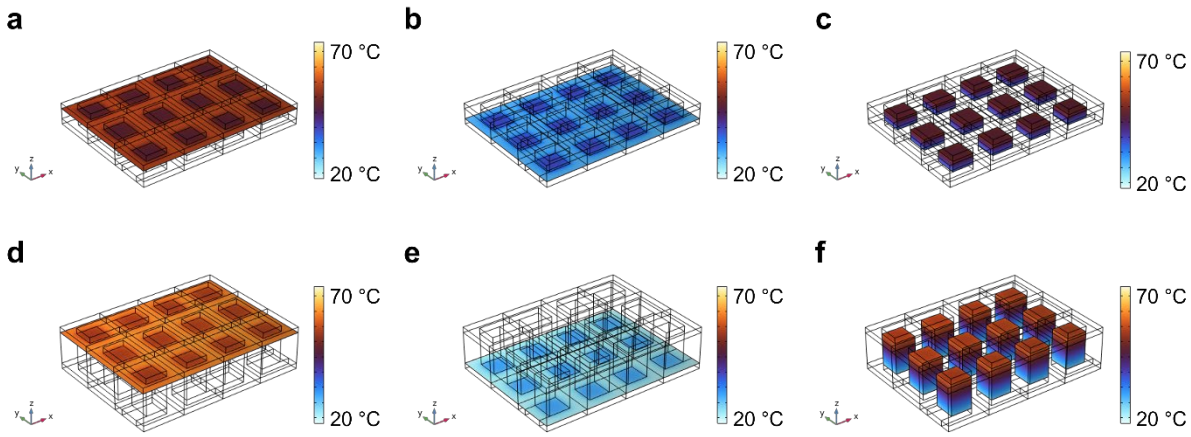

Supplementary Fig. 9 | Temperature distribution simulation of TE Lego block devices using COMSOL

Temperature distribution of **a.** upper part, **b.** lower part and **c.** TE leg parts with low aspect ratio of TE legs and **d.** upper part, **e.** lower part and **f.** TE leg parts with high aspect ratio of TE legs

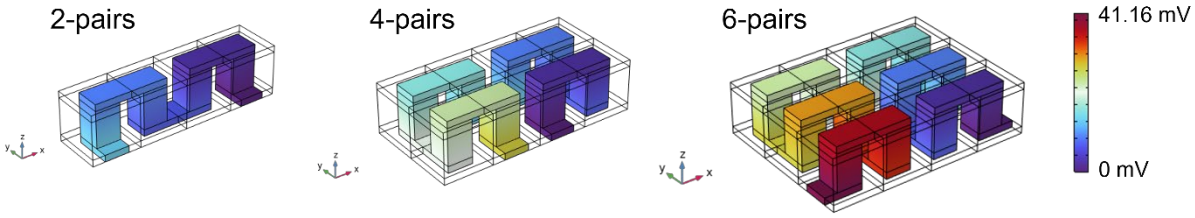

Supplementary Fig. 10 | Output voltage simulation of 2, 4 and 6 pairs of TE Lego block devices using COMSOL

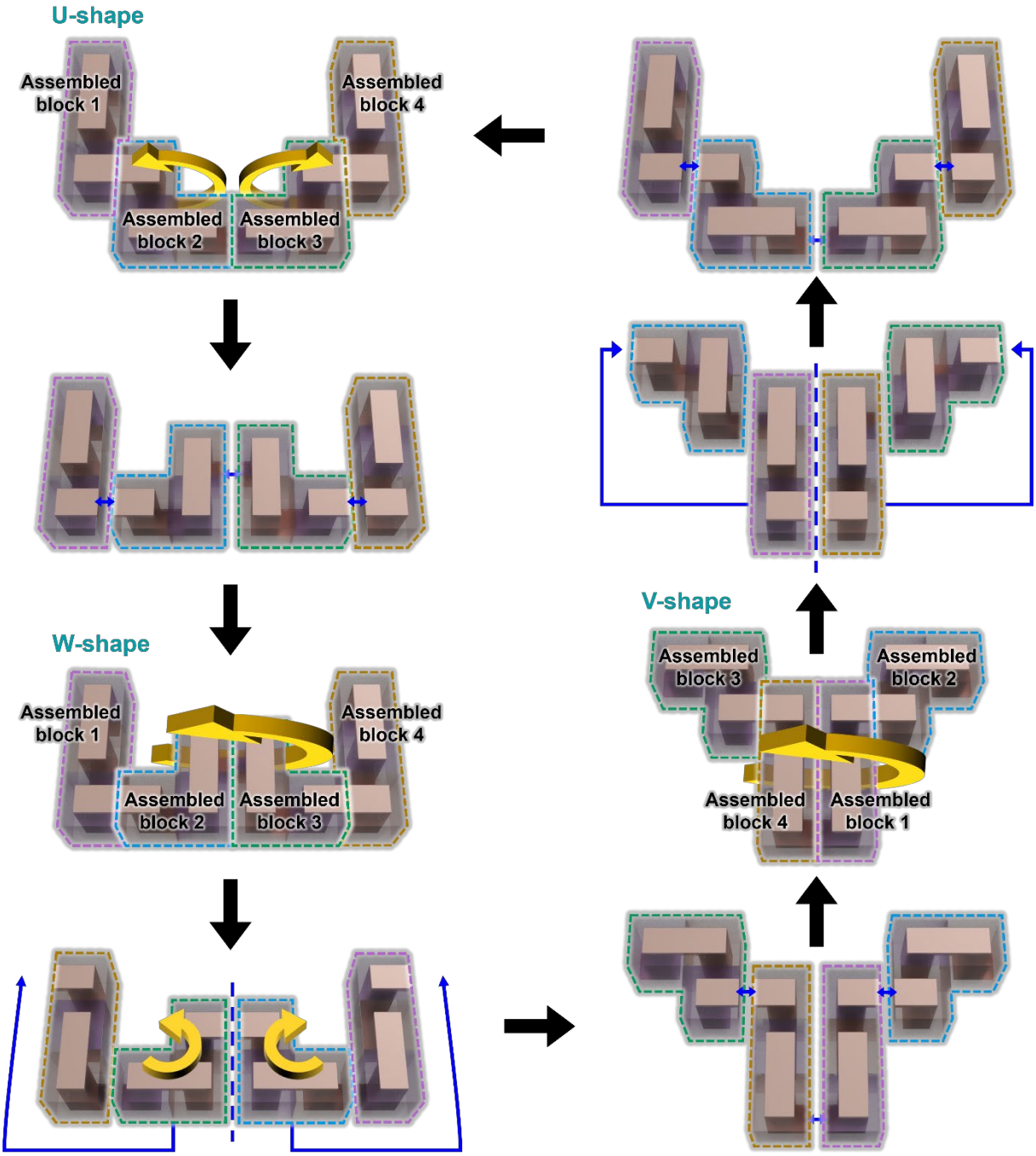

Supplementary Fig. 11 | Reconfiguring method of U-, V- and W-shaped TE Lego block devices

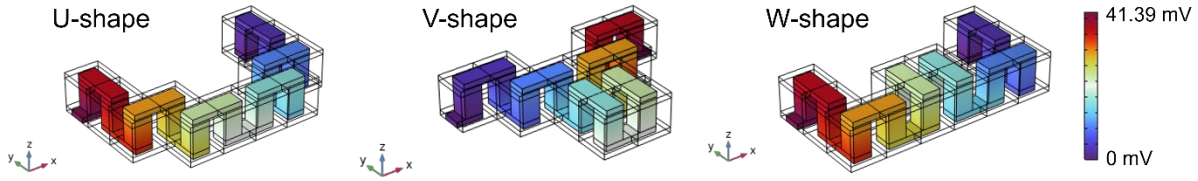

Supplementary Fig. 12 | Output voltage simulation of U-, V-, W-shaped TE Lego block devices using COMSOL